Evaporative Thinning: A Facile Synthesis Method for High Quality Ultrathin Layers of 2D Crystals

Yi-Kai Huang,[†,#] Jeffrey D. Cain,[†,#] Lintao Peng,[‡,§] Shiqiang Hao,[†] Thomas Chasapis,[∥] Mercouri G. Kanatzidis,[∥] Christopher Wolverton,[†] Matthew Grayson,[‡,§] and Vinayak P. Dravid*[,†,§]

[†]Department of Materials Science and Engineering, [‡]Department of Electrical Engineering and Computer Science, [§]Department of Applied Physics, and [∥]Department of Chemistry, Northwestern University, Evanston, Illinois 60208, United States. [#]Yi-Kai Huang and Jeffrey D. Cain contributed equally.

ABSTRACT The palette of two-dimensional materials has expanded beyond graphene in recent years to include the chalcogenides among other systems. However, there is a considerable paucity of methods for controlled synthesis of mono- and/or few-layer two-dimensional materials with desirable quality, reproducibility, and generality. Here we show a facile top-down synthesis approach for ultrathin layers of 2D materials down to monolayer. Our method is based on controlled evaporative thinning of initially large sheets, as deposited by vapor mass-transport. Rather than optimizing conditions for monolayer deposition, our approach makes use of selective evaporation of thick sheets to control the eventual thickness, down to a monolayer, a process which appears to be self-stopping. As a result, 2D sheets with high yield, high reproducibility, and excellent quality can be generated with large (>10 μm) and thin (~1−2 nm) dimensions. Evaporative thinning promises to greatly reduce the difficulty involved in isolating large, mono- and few-layers of 2D materials for subsequent studies.

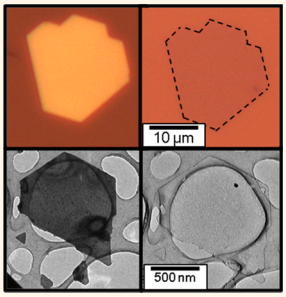

KEYWORDS: two-dimensional (2D) materials · 2D synthesis · bismuth selenide · transmission electron microscopy

Recently, two-dimensional (2D) materials have attracted a great deal of attention because of their exotic fundamental properties and potential for novel applications.[1−6] Following the success of graphene, the scientific community has developed interests in the exploration of other 2D materials such as h-BN,[7,8] MoS_2,[9,10] GaS,[11] WSe_2,[12] and Bi_2Se_3[13,14] among others. To study new 2D materials efficiently, a generic, high-yield synthesis process is desired with the capability of reliably producing few layer flakes (<5 nm) with large lateral dimensions (>10 μm) while maintaining good crystalline quality.

Mechanical exfoliation is the traditional method for synthesis of 2D materials, as first demonstrated by Novoselov *et al.*[15] with graphene. Mechanical exfoliation renders flakes of high quality representative of the bulk, but has the drawback of low yield and the requirement of single (or large grained) crystal specimens. Chemical and solution exfoliation have much higher yields than the mechanical exfoliation method, but result in flakes with high defect density and, in the case of MoS_2, potential phase transformation. Furthermore, this technique has not been proven to be effective on other 2D systems.

Recently, there have been reports of using catalyst-free vapor-transport to grow 2D materials.[13,16] This method results in high quality flakes without the low-yield of mechanical exfoliation and is particularly well suited for the growth of 2D materials. This method also comes with its disadvantages; as the thicknesses of these flakes decrease, so too do the lateral dimensions. For flakes thinner than ~10 nm, their sizes are generally on the order of 1−5 μm, too small for many characterization techniques. Herein we report a top down, evaporative thinning technique for the synthesis of ultrathin layers of 2D materials, down to monolayer thickness. We demonstrate retention of flake integrity and phase purity. The technique is demonstrated for Bi_2Se_3 and Sb_2Te_3, but our results indicate that it may apply to many other systems that are amenable to evaporation or sublimation. There are two isolated reports on thermal etching of mechanically exfoliated MoS_2 flakes, which

* Address correspondence to v-dravid@northwestern.edu.

Received for review August 19, 2014 and accepted September 18, 2014.

Published online September 18, 2014
10.1021/nn504664p

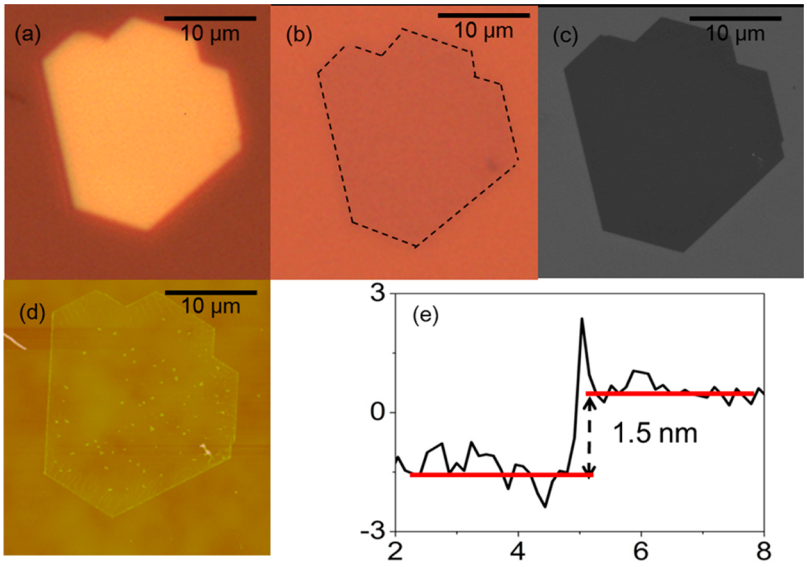

Figure 1. Images of a Bi_2Se_3 flake: (a) optical image before thinning; (b) optical image after thinning; (c) scanning electron microscope image after thinning; (d) AFM image after thinning; (e) AFM thickness profile of thinned flake.

either resulted in second phase formation or extensive flake damage.[17,18]

Bi_2Se_3 and Sb_2Te_3 are narrow bandgap layered semiconductors and thermoelectric materials which have recently been shown to be topological insulators (TI), a new electronic state of matter with conductive surface states and a potential platform for exotic physics.[19−21] Both materials consist of five atom quintuple-layers (QL) approximately 1 nm thick. While monolayer Bi_2Se_3 does not exhibit topological surface states,[21] the isolation of monolayers of these materials provides an excellent platform for studying TI surface chemistry, an issue of interest within the TI community.

Our process begins with the deposition of relatively thick (typically >1 μm) plates with large lateral dimensions (>10 μm) using catalyst-free vapor-transport. The as-deposited plates are then annealed to remove material in a controlled manner. Using this new evaporative thinning approach, we demonstrate the ability to controllably and reliably produce single and bilayer Bi_2Se_3 and Sb_2Te_3 flakes with lateral dimensions exceeding 10 μm, suitable for a variety of studies.

RESULTS AND DISCUSSION

The premise of the evaporative thinning technique is to first deposit laterally large (>10 μm) and thick (>1 μm) plates of a suitable layered material, then to controllably evaporate (sublime) layers of molecular species from the flake to reduce its thickness to a few nanometers by controlling time and temperature, but with no reduction in lateral dimensions. Supporting Information, Figure S2 shows low-magnification optical images of a Bi_2Se_3 sample before and after annealing. It can be easily noted that there is a dramatic change in thickness for some of the flakes, evidenced by the change in optical contrast. There are several findings of note: First, uniform thinning occurs mainly on plates with *c*-axis orientation (with respect to the substrate). The deposition conditions can be tuned to control flake orientation so that *c*-axis orientation dominates, this is due to the effects of surface energy and bonding strength anisotropy, as demonstrated in both this work and the literature.[12,14,19] The flakes that are not *c*-axis oriented, such as the left flake shown in Figure S2, are not uniformly thinned and thus form crumpled sheets or worm-like structures rather than flat sheets. There are several factors that influence this result. The weight of the sheet itself can drive the bending. Furthermore, because the sheet is highly flexible, the argon flow during the annealing process can also contribute to the shape-deformation. Certainly, the diminishment of substrate support can also make an effect here. Second, the quality of the resultant flake is most dependent on the annealing temperature. The optimal annealing temperature for the selenides and tellurides is between 60%−70% of the melting point. Third, the process time is highly dependent on the initial plate thickness. This fact is the reason there is a distribution of thicknesses in Figure S2. Additional experiments have shown that with long annealing times, nearly all flakes are reduced to mono- or bilayer.

Figure 1 shows higher magnification images (optical, AFM, SEM) along with the thickness profile of a Bi_2Se_3 flake before and after annealing at 510 °C. The flake is approximately 15 μm wide, with an initial thickness of 3.5 μm, as measured by profilometer. Following evaporative thinning, there is an obvious and visible contrast change, shown in Figure 1b, which is a typical indication of a reduction in thickness. Scanning electron microscopy (Figure 1c) confirms that the sheet is still intact and that it retains its pretreatment shape and

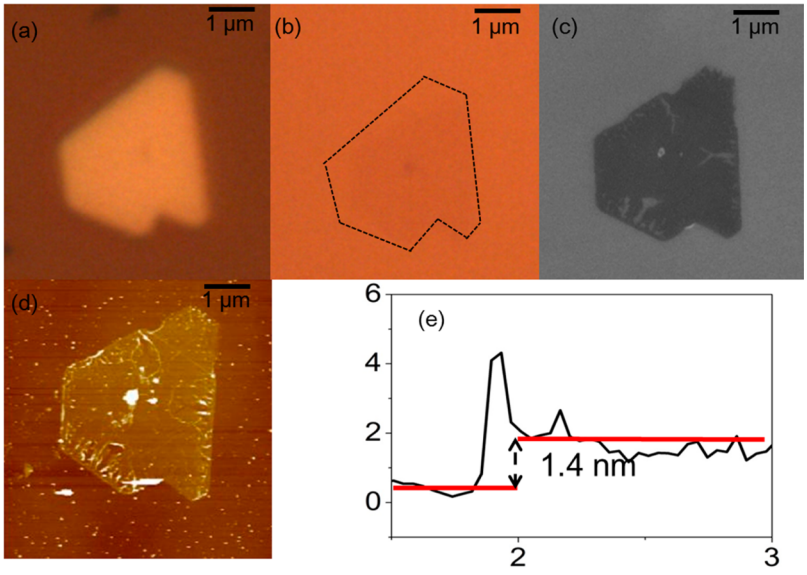

Figure 2. Images of a Sb_2Te_3 flake: (a) OM before thermal thinning. Panels b, c, and d are OM, SEM, and AFM height images after thermal thinning, respectively. (e) Height analysis from panel d.

lateral lengths. Figure 1 panels d and e show the AFM image and height profile. This confirms that the resultant flake is flat and has a thickness of approximately 1.5 nm (~1 QL). A small amount of wrinkling and folding is seen at the edges of the sheet with thicknesses of 3−5 nm. This is consistent with prior reports,[23] as folding has been seen in graphene sublimation. Analogous to the case of graphene, the folding and wrinkling is driven by the elevated temperatures and the need to reduce the number of dangling bonds at the flake edge. The small particles on the basal plane of the flake were probably formed through the same mechanism. Note, we do not see any difference in thinning behavior with regard to the lateral size of the initially deposited flake in the range of few a few micrometers to more than 50 μm. This is also confirmed in Supporting Information, Figure S6.

Similar to Bi_2Se_3, monolayer Sb_2Te_3 can be prepared in the same manner. Figure 2 shows images of a Sb_2Te_3 flake before and after thermal thinning along with the corresponding AFM thickness measurements. Because of the lower melting point of Sb_2Te_3, the thinning temperature was set at 490 °C. Similar to the case of Bi_2Se_3, the change in thickness was easily observed in optical microscope images by the change in optical contrast. SEM and AFM further confirmed the integrity of the flake and that the shape was preserved after thermal thinning. For Sb_2Te_3, flakes with thicknesses down to 1.4 nm (~1 QL) have been synthesized. It should be noted that the Sb_2Te_3 exhibits a greater degree of wrinkling and folding, an indication that the annealing temperature could potentially be reduced to yield even higher quality sheets.

To investigate the dynamics of evaporative thinning in real time and real-space, *in situ* TEM with a heating specimen holder was employed, as shown in Figure 3. These series of images were taken over the course of 15 min at 510 °C at two different locations on the TEM grid. As the time progresses at a given temperature, the flake becomes thinner, and thus more electron transparent. There are several important findings from this series of *in-situ* heating experiments. First, it is remarkable that the flakes evaporate while still retaining the faceted morphology, suggesting that both the evaporative molecular species and the remaining flake conform to the nominal Bi_2Se_3 composition. Second, the evaporation starts at the edge and propagates toward the center, which is expected given the presence of unterminated bonds at the edge. The flake remains flat and uniform, with no observable bending or bulging. Third, similar as the results from *ex-situ* heating shown in Figures 1 and 2, the lateral dimensions of the flake remain unchanged. During the evaporation process, the least favorable thing to happen is to have shrinkage in lateral size, but due to the 2D nature of the material, we observe the lateral size is nearly unchanged. This is a highly desired attribute of the evaporative thinning approach, since it allows making a uniform and large-size flake (>10 μm) to apply measurements, whereas the limitation in lateral size is always a drawback for the mechanical exfoliation technique. The final and most interesting observation is that the evaporation seems to have a self-limiting or self-stopping behavior. In Figure 3a, the upper section of the flake is much thinner than the lower section, seen from the electron transparency in the initial TEM image. If the evaporation rate were constant, one would expect the upper section to disappear as time passed, while the lower sections continue to be thinned. However, both sections are reduced to the same thickness and evaporation ceases (or is drastically reduced). Moreover, after the thickness was reduced

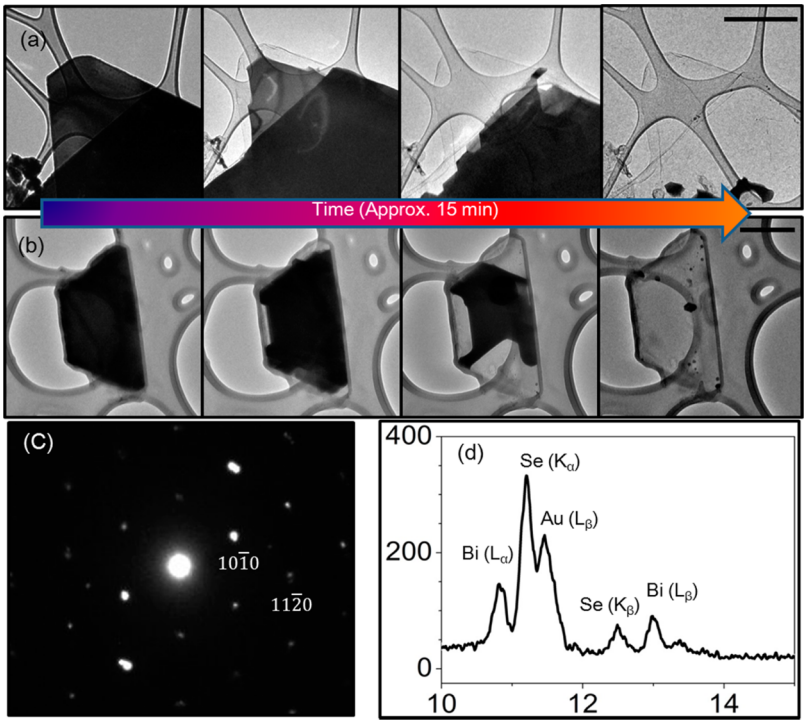

Figure 3. *In-situ* **TEM results of Bi_2Se_3 on lacey carbon TEM grid. (a and b) Thickness of flakes is systematically reduced over time at 510 °C. (c) Electron diffraction pattern of a thin flake. (d) EDS spectrum of a thin flake. Images were taken at 80 kV acceleration voltage, while EDS was taken at 120 kV. Scale bar is 500 nm.**

to complete electron transparency, the heating continued for an additional 15 min and the entire flake survived intact. This suggests a self-stopping nature of our evaporative thinning approach. The *in situ* TEM heating experiments also clarify that the substrate plays a minimal role in the self-stopping behavior, since the TEM grid used is lacey carbon, which provides very little support.

This self-stopping phenomenon was also observed during other evaporative thinning experiments. Following the initial vapor−solid deposition, each flake was over a micrometer in thickness, and it can be assumed that none are of exactly the same thickness. Therefore, if the evaporation rate were constant during heat treatment there should be one monolayer remaining, while the rest disappear (over thinned) or are still thick (under thinned). However, many mono and few-layer samples are commonly seen after evaporative thinning. For example, in Supporting Information, Figure S2 there is more than one few-layer flakes remaining. The evaporative thinning experiments and the *in situ* TEM heating experiments support the hypothesis that our process is self-stopping. This self-limiting mechanism greatly simplifies the thinning procedure because the optimal heating time window is widened and the yield is greatly improved.

We present two plausible mechanisms for this phenomenon. First, as shown for graphene,[23] the edge folding and scroll formation during evaporation stabilizes the flake-edge against heat treatment. From Figure 3, we can see the thinning starts from the edge of the flake and moves inward. The folding at the edges of the Bi_2Se_3 flake stabilizes the edge by reducing the number of dangling bonds, thus making the entire flake more robust against bond-breaking and evaporation. A slight increase in thickness at the edges of our samples is observed in the AFM thickness profiles, which we attribute to folding at the edge.

The second possibility is the potential difference in the melting point between the bulk and single layer. As shown for graphene, the melting point increases by approximately 300 K compared to graphite,[22] making evaporation/sublimation more difficult. To verify if this phenomenon also applies to chalcogenides, we performed first-principles atomistic simulations. The Lindemann criterion was proposed to predict the bulk melting point of crystalline materials.[24,25] The idea behind this theory is the observation that the average amplitude of thermal vibrations increases with increasing temperature. The Lindemann criterion states that melting is expected when the root-mean-square vibration amplitude exceeds a threshold value,[22] $\gamma_{bulk} = (\langle u^2 \rangle_m)^{1/2}/d \cong 0.2$, where $\langle u^2 \rangle_m$ is the mean square displacement at melting temperature and d is the nearest neighbor interatomic distance at 0 K. It is known that the mean square displacement in 2D materials is not an appropriate measure to distinguish between the solid and the liquid phases, since it diverges at long times with increasing system size.[26,27]

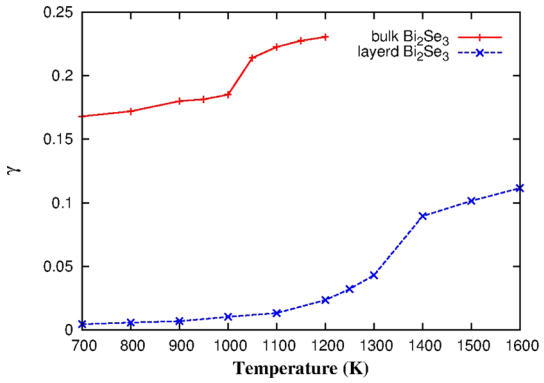

Figure 4. Lindemann criterion as a function of temperature for bulk and layered Bi_2Se_3. When the average root-mean-square vibration amplitude exceeds a certain threshold (e.g., 20% of the nearest neighbor distance) the melting process initiates.

Alternatively, the melting criterion is replaced by the relative displacement of neighboring particles (indices j and $j+1$)[25] $\gamma_{2D} = \langle(\mu_j - \mu_{j+1})^2\rangle/d^2$ where μ_j and μ_{j+1} are the neighboring atomic positions, and d is the nearest neighbor interatomic distance at 0 K. To get the atomic trajectories, we use ab initio Molecular Dynamics methods as implemented in VASP.[28] We use 160 and 125 atom supercells for bulk and single layered Bi_2Se_3, respectively. The trajectories are recorded for the systems over 2 ps under an NVT ensemble. In Figure 4, we show the melting criteria for bulk and layered Bi_2Se_3. As we can see, there is an abrupt change for bulk Bi_2Se_3 around 1000−1050 K, and an abrupt change for layered Bi_2Se_3 around 1300−1400 K; we hence identify the melting temperatures to be 1050 and 1400 K for bulk and layered Bi_2Se_3, respectively. The calculated bulk melting temperature 1050 K is slightly higher than the experimental melting temperature 980 K. Similarly, the melting points for bulk and layered Sb_2Te_3 are identified as 950 and 1200 K, shown in Supporting Information, Figure S4. The calculated bulk melting temperature 950 K is also slightly higher than the experimental measurement of 853 K. This could potentially explain the self-limiting behavior seen with Bi_2Se_3. The thinning stops when the flake reaches single (or few) layer due to the increase in melting point, which makes the flake more robust against sublimation.

The diffraction pattern in Figure 3c demonstrates that the flake is still single crystalline and possesses the 6-fold projected symmetry characteristic of the Bi_2Se_3 crystal structure after evaporative thinning. The calculated lattice spacing is 4.21 Å, which matches well with the reported value of 4.14 Å. It should be noted that the diffraction pattern is not exactly on zone; this is because the flake has shifted or rotated during the heating process due to a lack of rigid support. Figure 3d shows the EDS spectrum which exhibits both bismuth and selenium peaks. The Au peak comes from the TEM grid. The biggest potential concern with our process is whether or not the final product is still stoichiometric Bi_2Se_3, and the results in Figure 3 panels c and d confirm that it is.

Similar *in situ* TEM heating measurements were conducted for Sb_2Te_3 and the results are shown in Supporting Information, Figure S3. The evaporative thinning behavior is similar to Bi_2Se_3; the flakes retain their preprocessing shape, the evaporation starts from the edge, and the process is, once again, self-stopping. These shared characteristics demonstrate that this method could potentially be applied to a variety of layered materials that are conducive to evaporation/sublimation of molecular species. Because of the lower melting point of Sb_2Te_3 (580 °C) compared to that of Bi_2Se_3 (710 °C), the thinning process started at as low as 450 °C, and the thin flake (*ca.* 1−2 nm) tended to become porous at temperatures over 525 °C.

As mentioned above, temperature appears to be the most important parameter in the evaporative thinning process. Supporting Information, Figure S5 shows the evolution of a microstructure at different thinning temperatures. All three samples were processed under the same conditions with the exception of temperature. At 400 °C the Bi_2Se_3 flake had etching pits on its surface, which had triangular or hexagonal geometry. This is consistent with the *in situ* TEM results at the early stages of heating. At optimal temperature, the flake was relatively uniform, while at even higher temperature, the flake started to break up and the integrity of the flake was compromised forming worm-like structures. Such worm-like or buckyball structures are more stable against breakdown at higher temperatures.[23]

According to the proposed evaporative thinning mechanism discussed earlier, the thinning behavior should not be related to how the flake is deposited on the substrate but only its postdeposition treatment. Therefore, the traditional "scotch-tape" method was employed to make Bi_2Se_3 flakes on Si/SiO_2 substrate followed by thermal processing. The results are shown in Supporting Information, Figure S6, where the difference in thickness is clearly seen by the change in optical contrast. Other than reducing the thickness of the exfoliated flakes, this method has the additional advantage of removing the organic residue left by the scotch-tape which can contaminate the deposited material.

Charge transport measurements were performed on a single layer (1 nm) Bi_2Se_3 device with a back gate. Electrodes were patterned and deposited by standard e-beam lithography and thermal evaporation. It has been shown that Bi_2Se_3 can be oxidized in ambient condition,[29] and in fact we observed change in the transport properties of the flakes after putting the sample in air for more than a month. Therefore, to remove surface contamination, the device with metal electrodes (Figure 5 right inset) was annealed in a reducing chamber at 130 °C with flowing forming

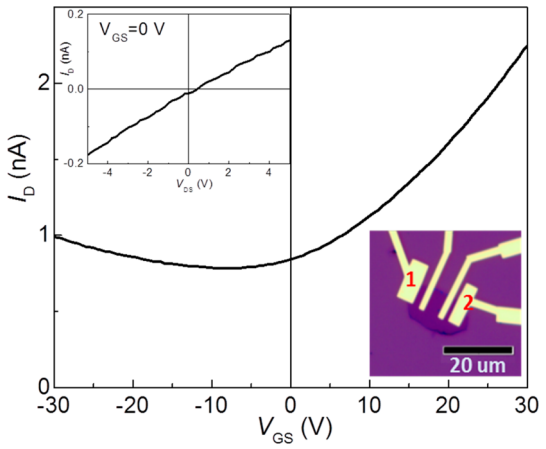

Figure 5. Gate-dependent drain current I_D from a single QL Bi_2Se_3 device (right inset) with V_{DS} = 30 V and a minima at V_{DS} = −9 V. Left inset shows the I−V curve of the same device at V_{GS} = 0 V.

gas (5% H_2 in N_2) while the pressure was held constant at −5 psi for 5 h. The device was then cooled down to room temperature sitting in vacuum for another 6 h. The I−V curve (Figure 5 left inset) with drain voltage bias from −5 to 5 V with zero gate bias shows good linearity, confirming the Ohmic contact. The sheet resistance calculated from its slope is about 46.5 G-ohms. It should be noted that although Bi_2Se_3 is a topological insulator, it has been confirmed that this property disappears when flake thickness is below 5 nm,[21] and that likely explains the high resistance in our device compared to the bulk sample. Figure 5 shows a gate-dependent drain current I_D at a drain voltage bias of 30 V. The nominal charge neutrality voltage at the conductivity minima is V_0 = −9 V. The increased conductance at more negative biases $V < V_0$ implies p-type in that range, and increased conductance at more positive biases $V > V_0$ implies n-type in that range. The resistance is consistent with prior work on ultrathin Bi_2Se_3,[30] and further confirms the quality of the flakes synthesized using this method. The availability of high quality monolayer flakes of Bi_2Se_3 and other materials using the evaporative thinning technique described above promises to provide an excellent platform to investigate TI surface physics and the effects of gas adsorption on their electronic properties.

SUMMARY AND CONCLUSIONS

Evaporative thinning enables a facile, widely accessible, potentially broadly deployable method for the synthesis of high-quality ultrathin layers of 2D materials. The effect allows the controlled removal of material where entire layers are removed without a reduction in the lateral dimensions of the remaining layers, as demonstrated for Bi_2Se_3 and Sb_2Te_3. Specifically, large (>10 μm), thin (1−2 nm), and high quality chalcogenide flakes can be synthesized with high yield, which serves as a platform to study 2D materials. Other than its promising applications on future study of 2D materials, the method itself shows interesting scientific phenomena. The self-stopping mechanism is first reported in literature and it manifests the uniqueness of monolayer materials.

EXPERIMENTAL METHODS

Crystals of Bi_2Se_3 and Sb_2Te_3 were synthesized by melting the appropriate ratios of high purity (5 nine) starting materials Bi, Se, and Sb, Te, respectively. The starting materials were sealed in evacuated quartz tubes (~10^{-4} Torr) and heated to 850 °C over the course of 15 h and held at this temperature for 10 h with periodic shaking to ensure compositional homogeneity. The samples were then cooled to room temperature over 15 h. Powder diffraction patterns of pulverized final materials were obtained using a Cu Kα (λ = 1.548 Å) radiation in a reflection geometry on an Inel diffractometer equipped with a position sensitive detector and operating at 40 kV and 20 mA. The experimental Bragg reflections shown in Supporting Information, Figure S1a,b confirmed that the compositions are single phase materials and can be well indexed with the rhombohedral structure. The lattice constants obtained after powder XRD refinement are a = 4.138 Å and c = 28.624 Å for Bi_2Se_3 and a = 4.264 Å c = 30.443 Å for Sb_2Te_3.

Following the synthesis of bulk Bi_2Se_3 and Sb_2Te_3, large Bi_2Se_3 and Sb_2Te_3 plates were deposited using a catalyst-free vapor-transport method. An alumina boat containing the powdered source material was positioned in the hot center of a 12″ Lindberg Blue tube furnace with a 1″ silica tube. Si substrates covered in a 300 nm SiO_2 layer were placed downstream in a colder zone within the furnace (approximately 8 cm from hot center). For Bi_2Se_3, the chamber pressure was maintained at approximately 10 Torr with an ultrahigh purity Ar flowing in at 25 sccm. The furnace was heated to 570 °C over the course of 35 min and held at that temperature for 15 min before cooling naturally over the course of 1 h. For Sb_2Te_3, The chamber pressure was held at approximately 5 Torr with a flow rate of 25 sccm. The furnace was heated to 485 °C over the course of 30 min and held at that temperature for 15 min before cooling naturally.

After the initial deposition of Bi_2Se_3 or Sb_2Te_3, the substrates covered with large crystalline plates were positioned in the hot center of the tube furnace and held at 490 °C for 10 min for Sb_2Te_3, and 510 °C for 10 min for Bi_2Se_3. After the prescribed time, the entire silica tube is removed from the furnace in order to cool rapidly. The chamber is held at 20 Torr with 20 sccm of flowing Ar during evaporation for both materials.

To prepare samples suitable for TEM analysis, Bi_2Se_3 or Sb_2Te_3 were first deposited onto single crystal NaCl substrates using the same growth conditions described above. The NaCl substrates were then dissolved in a small amount of deionized water and the flakes were scooped out using a lacey carbon TEM grid. The grid was then air-dried on filter paper in a sealed container. The specimen was mounted on an *in situ* heating TEM holder and heated to 510 °C over 5 min. To minimize the damaging effects of the electron beam, all imaging was done at 80 kV acceleration voltage and under beam blanked and reduced current modes.

Conflict of Interest: The authors declare no competing financial interest.

Supporting Information Available: Detailed information on material characterization and microscopy, X-ray diffraction pattern of starting powders, additional *in situ* TEM images of Sb_2Te_3, additional computational results for Sb_2Te_3, and additional

optical microscopy images of thinned Sb_2Te_3. This material is available free of charge *via* the Internet at http://pubs.acs.org.

Acknowledgment. This work was supported by the National Science Foundation's MRSEC program (DMR-1121262) and made use of its Shared Facilities at the Materials Research Center of Northwestern University. This work made use of the EPIC facility (NU*ANCE* Center-Northwestern University), which has received support from the MRSEC program (NSF DMR-1121262) at the Materials Research Center, The Nanoscale Science and Engineering Center (EEC-0118025/003), both programs of the National Science Foundation; the State of Illinois; and Northwestern University. J.C. is supported by the Department of Defense (DoD) through the National Defense Science and Engineering Fellowship (NDSEG) Program. S.H. and C.W. gratefully acknowledge support from DOE under Grant No. DE-FG02-07ER46433.

REFERENCES AND NOTES

1. Schedin, F.; Geim, A. K.; Morozov, S. V.; Hill, E. W.; Blake, P.; Katsnelson, M. I.; Novoselov, K. S. Detection of Individual Gas Molecules Adsorbed on Graphene. *Nat. Mater.* **2007**, *6*, 652–655.
2. Geim, A. K.; Novoselov, K. S. The Rise of Graphene. *Nat. Mater.* **2007**, *6*, 183–191.
3. Shanmugam, M.; Bansai, T.; Durcan, C. A.; Yu, B. Molybdenum Disulphide/Titanium Dioxide Nanocomposite-poly 3-hexylthiophene Bulk Heterojunction Solar Cell. *Appl. Phys. Lett.* **2012**, *100*, 153901.
4. Han, T. H.; Huang, Y.; Tan, A.; Dravid, V.; Huang, J. Steam Etched Porous Graphene Oxide Network for Chemical Sensing. *J. Am. Chem. Soc.* **2011**, *133*, 15264–15267.
5. Late, D. J.; Huang, Y.; Liu, B.; Acharya, J.; Shirodkar, S. N.; Luo, J.; Yan, A.; Charles, D.; Waghmare, U. V.; Dravid, V. P.; *et al*. Sensing Behavior of Atomically Thin-Layered MoS_2 Transistors. *ACS Nano* **2013**, *7*, 4879.
6. Rao, C. N. R.; Ramakrishna Matte, H. S. S.; Maitra, U. Graphene Analogues of Inorganic Layered Materials. *Angew. Chem., Int. Ed.* **2013**, *52*, 13162.
7. Nag, A.; Raidongia, K.; Hembram, K.; Datta, R.; Waghmare, U. V.; Rao, C. N. R. Graphene Analogues of BN: Novel Synthesis and Properties. *ACS Nano* **2010**, *4*, 1539–1544.
8. Gorbachev, R. V.; Riaz, I.; Nair, R. R.; Jalil, R.; Britnell, L.; Belle, B. D.; Hill, E. W.; Novoselov, K. S.; Watanabe, K.; Taniguchi, T.; *et al*. Hunting for Monolayer Boron Nitride: Optical and Raman Signatures. *Small* **2011**, *7*, 465–468.
9. Splendiani, A.; Sun, L.; Zhang, Y.; Li, T.; Kim, J.; Chim, C.; Galli, G.; Wang, F. Emerging Photoluminescence in Monolayer MoS_2. *Nano Lett.* **2010**, *10*, 1271–1275.
10. Zhang, W.; Chuu, C.; Huang, J.; Chen, C.; Tsai, M.; Chang, Y.; Liang, C.; Chen, Y.; Chueh, Y.; He, J.; I; *et al*. Ultrahigh-Gain Photodetectors Based on Atomically Thin Graphene-MoS_2 Heterostructures. *Sci. Rep.* **2014**, *4*, 3826.
11. Late, D. J.; Liu, B.; Luo, J.; Yan, A.; Matte, H. S. S. R.; Grayson, M.; Rao, C. N. R.; Dravid, V. P. GaS and GaSe Ultrathin Layer Transistors. *Adv. Mater.* **2012**, *24*, 3549–3554.
12. Fang, H.; Chuang, S.; Chang, T. C.; Takei, K.; Takahashi, T.; Javey, A. High-Performance Single Layered WSe_2 p-FETs with Chemically Doped Contacts. *Nano Lett.* **2012**, *12*, 3788–3792.
13. Kong, D. S.; Dang, W. H.; Cha, J. J.; Li, H.; Meister, S.; Peng, H. L.; Liu, Z. F.; Cui, Y. Few-Layer Nanoplates of Bi_2Se_3 and Bi_2Te_3 with Highly Tunable Chemical Potential. *Nano Lett.* **2010**, *10*, 2245–2250.
14. Jana, M. K.; Biswas, K.; Rao, C. N. R. Ionothermal Synthesis of Few-Layer Nanostructures of Bi_2Se_3 and Related Materials. *Chem.—Eur. J.* **2013**, *19*, 9110.
15. Novoselov, K. S.; Geim, A. K.; Morozov, S. V.; Jiang, D.; Zhang, Y.; Dubonos, S. V.; Grigorieva, I. V.; Firsov, A. A. Electric Field Effect in Atomically Thin Carbon Films. *Science* **2004**, *306*, 666–669.
16. Dang, W.; Peng, H.; Li, H.; Wang, P.; Liu, Z. Epitaxial Heterostructures of Ultrathin Topological Insulator Nanoplate and Graphene. *Nano Lett.* **2010**, *10*, 2870–2876.
17. Lu, X.; Utama, M. I. B.; Zhang, J.; Zhao, Y.; Xiong, Q. Layer-By-Layer Thinning of MoS_2 by Thermal Annealing. *Nanoscale* **2013**, *5*, 8904–8908.
18. Wu, J.; Li, H.; Yin, Z.; Li, H.; Liu, J.; Cao, X.; Zhang, Q.; Zhang, H. Layer Thinning and Etching of Mechanically Exfoliated MoS_2 Nanosheets by Thermal Annealing in Air. *Small* **2013**, *9*, 3314–3319.
19. Zhang, Y.; He, K.; Chang, C. Z.; Song, C. L.; Wang, L. L.; Chen, X.; Jia, J. F.; Fang, Z.; Dai, X.; Shan, W. Y.; *et al*. Crossover of the Three-Dimensional Topological Insulator Bi_2Se_3 to the Two-Dimensional Limit. *Nat. Phys.* **2010**, *6*, 584–588.
20. Steinberg, H.; Gardner, D. R.; Lee, Y. S.; Jarillo-Herrero, P. Surface State Transport and Ambipolar Electric Field Effect in Bi_2Se_3 Nanodevices. *Nano Lett.* **2010**, *10*, 5032–5036.
21. Peng, H. L.; Dang, W. H.; Cao, J.; Chen, Y. L.; Wu, W.; Zheng, W. S.; Li, H.; Shen, Z. X.; Liu, Z. F. Topological Insulator Nanostructures for Near-Infrared Transparent Flexible Electrodes. *Nat. Chem.* **2012**, *4*, 281–286.
22. Zakharchenko, K. V.; Fasolino, A.; Los, J. H.; Katsnelson, M. I. Melting of Graphene: From Two to One Dimension. *J. Phys.: Condens. Matter* **2011**, *23*, 202202.
23. Huang, J. Y.; Ding, F.; Yakobson, B. I.; Lu, P.; Qi, L.; Li, J. *In Situ* Observation of Graphene Sublimation and Multi-layer Edge Reconstructions. *Proc. Natl. Acad. Sci. U.S.A.* **2009**, *106*, 10103–10108.
24. March, N. H.; Tosi, M. P. *Introduction to Liquid State Physics*; World Scientific: Singapore, 2002.
25. Ziman, J. M. *Principles of the Theory of Solids*; Cambridge University Press: Cambridge, UK, 1972.
26. Landau, L. D.; Lifshitz, E. M. *Statistical Physics*; Pergamon: Oxford, UK, 1980.
27. Zahn, K.; Maret, G. Dynamic Criteria for Melting in Two Dimensions. *Phys. Rev. Lett.* **2000**, *85*, 3656.
28. Kresse, G.; Furthmuller, J. Efficiency of ab-Initio Total Energy Calculations for Metals and Semiconductors Using a Plane-Wave Basis Set. *Comput. Mater. Sci.* **1996**, *6*, 15–50.
29. Kong, D. S.; Cha, J. J.; Lai, K. J.; Peng, H. L.; Analytis, J. G.; Meister, S.; Chen, Y. L.; Zhang, H. J.; Fisher, I. R.; Shen, Z. X.; Cui, Y. Rapid Surface Oxidation as a Source of Surface Degradation Factor for Bi_2Se_3. *ACS Nano* **2011**, *5*, 4698–4703.
30. Hong, S. S.; Kundhikanjana, W.; Cha, J. J.; Lai, K.; Kong, D.; Meister, S.; Kelly, M. A.; Shen, Z.; Cui, Y. Ultrathin Topological Insulator Bi_2Se_3 Nanoribbons Exfoliated by Atomic Force Microscopy. *Nano Lett.* **2010**, *10*, 3118–3122.